Exchange effects in nucleus-nucleus reactions

J. Dohet-Eraly [1,2,*] and P. Descouvemont [2,†]

[1] *Physique Quantique, C.P. 165/82, Université Libre de Bruxelles (ULB), B 1050 Brussels, Belgium*

[2] *Physique Nucléaire Théorique et Physique Mathématique, C.P. 229, Université Libre de Bruxelles (ULB), B 1050 Brussels, Belgium*

(Received 16 October 2020; revised 12 January 2021; accepted 11 March 2021; published 25 March 2021)

We present a scattering model for nuclei with similar masses. In this three-body model, the projectile has a core+valence structure, whereas the target is identical to the core nucleus. The three-body wave functions must be symmetrized for the exchange of the cores. This property gives rise to nonlocal potentials, which are computed without approximation. The present model is an extension of the continuum discretized coupled channel formalism, with an additional treatment of core exchange. We solve the coupled-channel system, including nonlocal terms, by the *R*-matrix method using Lagrange functions. This model is applied to the $^{13}C + ^{12}C$, $^{13}N + ^{12}C$, and $^{16}O + ^{12}C$ systems. Experimental scattering cross sections are fairly well reproduced without any parameter fitting. The backward-angle enhancement of the elastic cross sections is due to the nonlocal potential. We discuss in more detail the various nonlocal contributions and present effective local potentials.

DOI: 10.1103/PhysRevC.103.034619

I. INTRODUCTION

Nucleus-nucleus reactions represent an important topic in nuclear physics. In particular, they constitute the only way to investigate exotic nuclei. With the development of radioactive beams, more and more data become available. Accurate theoretical models are needed to interpret these data and to extract the relevant properties of exotic nuclei.

A popular approach is the optical model [1,2], where the structure of the colliding nuclei is neglected. Microscopic effects and absorption channels are simulated by complex potentials. This approach is very simple, but usually involves several parameters. Information about the structure of the nuclei is therefore limited.

Three-body models represent a step further in the description of nucleus-nucleus collisions. One of the participating nuclei is described by a two-body structure, and the main part of the absorption is simulated by breakup effects in this two-body nucleus. This approach is referred to as the continuum discretized coupled channel (CDCC) method [3–6], and has been extended to systems involving four-body systems [7,8]. It is well adapted to nuclei with a low separation energy, where breakup effects are expected to be important. The CDCC method was originally developed to describe deuteron scattering [3], but many applications have been performed recently for reactions involving exotic nuclei (see, e.g., Refs. [9,10] for recent works).

In its present form, the CDCC method neglects possible exchange effects between the projectile and the target. A typical example is the $\alpha + ^8$Be reaction [11], where the symmetrization between the colliding α particle and the α's involved in ^{8}Be is not taken into account. A more recent example is the $d + ^{11}$Be system [12], where d and ^{11}Be are described by $p + n$ and ^{10}Be $+n$ structures, without antisymmetrization between the neutrons of d and of ^{11}Be.

An obvious situation where exchange effects are important is when the colliding nuclei have similar masses. Representative examples are the $^{13}C + ^{12}C$ and $^{17}O + ^{16}O$ reactions. In such a case the system can be described by a three-body structure involving two cores and an exchanged particle (typically a nucleon or an α particle). The symmetrization of the wave function for the core exchange is then crucial. In the literature, several works have been done in this direction, with various approximations of the exchange effects [13–16].

In the present work, we use a three-body model, and treat exchange effects exactly. This procedure gives rise to nonlocal potentials in a coupled-channel formalism, but does not require any parameter fit. As in the traditional CDCC approach, the only inputs are the two-body interactions between the constituents. A first important step is to determine the nonlocal potentials, stemming from exchange effects. In a second step, one has to solve a coupled-channel integrodifferential system. This is in general a complicated task, but can be simplified with the help of the *R*-matrix formalism [17] associated with the Lagrange-mesh technique [18].

The paper is organized as follows. In Sec. II, we present the model, with emphasis on the calculation of the nonlocal terms. Section III is devoted to some applications. We present results on $^{13}C + ^{12}C$, $^{13}N + ^{12}C$, and $^{16}O + ^{12}C$ scattering. In Sec. IV, we discuss nonlocal effects in more detail. We focus on the long-range part of the nonlocal kernels. We also present equivalent local potentials. Concluding remarks and outlook are presented in Sec. V.

II. THE THREE-BODY MODEL

A. Total wave functions

We consider the three-body system presented in Fig. 1. The projectile is formed by a core (C) + valence (v) system,

*jdoheter@ulb.ac.be

†pdesc@ulb.ac.be

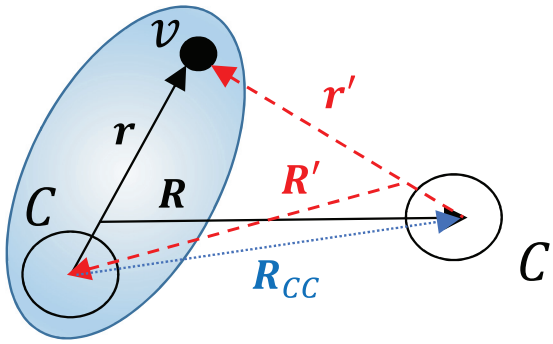

FIG. 1. Coordinates $(\boldsymbol{r}, \boldsymbol{R})$ and $(\boldsymbol{r}', \boldsymbol{R}')$. C and v represent the core and valence particles.

and the target is identical to the core. A typical example is the $^{13}\mathrm{C}+^{12}\mathrm{C}$ system, where the core is $^{12}\mathrm{C}$ and the valence particle a neutron. For the sake of simplicity, we assume that the spin of the core is zero. The Hamiltonian of this system is defined as

$$H = T_r + T_{\boldsymbol{R}} + V_{Cv}(\boldsymbol{r}) + V_{Cv}(|\alpha\boldsymbol{r} - \boldsymbol{R}|) + V_{CC}(|\beta\boldsymbol{r} + \boldsymbol{R}|), \quad (1)$$

where T_r and $T_{\boldsymbol{R}}$ are the kinetic energies associated with $\boldsymbol{r}$ and $\boldsymbol{R}$, and V_{Cv} and V_{CC} are core-valence and core-core potentials. The coordinates $\boldsymbol{R}$ and $\boldsymbol{R}'$ are the relative coordinates between the projectile and the target before and after symmetrization, respectively. In definition (1), α and β are positive coefficients given by

$$\alpha = \frac{A_C}{A_C + A_v}, \ \beta = \frac{A_v}{A_C + A_v} = 1 - \alpha, \quad (2)$$

where A_C and A_v are the masses of the core and of the valence particle, respectively. We also define

$$\gamma = \frac{1}{1 - \alpha^2}, \quad (3)$$

which will be used later.

The present approach is based on the CDCC formalism, but we include the symmetrization of the wave function with respect to core exchange. Notice that two possible choices exist for the potential V_{Cv}: either it reproduces the spectroscopic properties of the $C + v$ system, or it is fitted on elastic scattering.

Let us define the core-valence Hamiltonian by

$$H_0 = T_r + V_{Cv}(\boldsymbol{r}), \quad (4)$$

which is diagonalized from

$$H_0 \phi_n^{\ell jm}(\boldsymbol{r}) = E_n^{\ell j} \phi_n^{\ell jm}(\boldsymbol{r}). \quad (5)$$

The two-body wave functions are factorized as

$$\phi_n^{\ell jm}(\boldsymbol{r}) = \frac{u_n^{\ell j}(r)}{r} [Y_\ell(\Omega_r) \otimes \chi^v]^{jm}, \quad (6)$$

where χ^v is a spinor associated with the valence particle. The radial eigenfunctions $u_n^{\ell j}(r)$ are expanded over a basis, chosen here from Lagrange functions [18]. Lagrange-Laguerre functions regularized by r and by $\sqrt{r}$ [18,19] have been considered. Both provide the same level of accuracy. As usual in CDCC calculations, energies $E_n^{\ell j} < 0$ correspond to physical states, whereas states with $E_n^{\ell j} > 0$, referred to as pseudostates, simulate the projectile continuum.

The total wave functions, associated with Eq. (1) are written before symmetrization as

$$\Phi^{JM\pi}(\boldsymbol{R}, \boldsymbol{r}) = \frac{1}{R} \sum_{cL} g_{cL}^{J\pi}(R) \, \varphi_{cL}^{JM\pi}(\Omega_R, \boldsymbol{r}), \quad (7)$$

where index c stands for $c = (\ell jn)$ and where $g_{cL}^{J\pi}$ are radial wave functions to be determined. The relative angular momentum is denoted as L. The channel functions $\varphi_{cL}^{JM\pi}$ are defined as

$$\varphi_{cL}^{JM\pi}(\Omega_R, \boldsymbol{r}) = \left[Y_L(\Omega_R) \otimes \phi_n^{\ell j}(\boldsymbol{r})\right]^{JM}. \quad (8)$$

The total wave function (7) must be symmetrized with respect to the exchange of the cores. For spin-zero cores, this is achieved with the exchange operator P,

$$\Psi^{JM\pi}(\boldsymbol{R}, \boldsymbol{r}) = (1 + P)\Phi^{JM\pi}(\boldsymbol{R}, \boldsymbol{r}), \quad (9)$$

where P permutes the coordinates of the cores. More precisely, we have

$$P\Phi^{JM\pi}(\boldsymbol{R}, \boldsymbol{r}) = \Phi^{JM\pi}(\boldsymbol{R}', \boldsymbol{r}') \quad (10)$$

with

$$\boldsymbol{r}' = \alpha\boldsymbol{r} - \boldsymbol{R}, \quad \boldsymbol{R}' = (\alpha^2 - 1)\boldsymbol{r} - \alpha\boldsymbol{R}. \quad (11)$$

In the $(\boldsymbol{R}', \boldsymbol{r}')$ system, Hamiltonian (1) can be written, in the so-called "post" form, as

$$H = T_{r'} + T_{\boldsymbol{R}'} + V_{Cv}(\boldsymbol{r}') + V_{Cv}(|\alpha\boldsymbol{r}' - \boldsymbol{R}'|) + V_{CC}(|\beta\boldsymbol{r}' + \boldsymbol{R}'|). \quad (12)$$

In the next step, we consider the three-body Schrödinger equation

$$H\Psi^{JM\pi} = E\Psi^{JM\pi}, \quad (13)$$

and use Eq. (9) with expansion (7). After projection on the channel functions, this procedure provides the integrodifferential system

$$(T_R + E_c - E) g_{cL}^{J\pi}(R) + \sum_{c'L'} V_{cL,c'L'}^{J\pi}(R) g_{c'L'}^{J\pi}(R) + \sum_{c'L'} \int W_{cL,c'L'}^{J\pi}(R, R') g_{c'L'}^{J\pi}(R') dR' = 0, \quad (14)$$

where

$$T_R = -\frac{\hbar^2}{2\mu}\left[\frac{d^2}{dR^2} - \frac{L(L+1)}{R^2}\right], \quad (15)$$

μ being the reduced mass. The first two terms of Eq. (14) correspond to the standard CDCC system [5]. The coupling potentials are defined by

$$V_{cL,c'L'}^{J\pi}(R) = \left\langle \varphi_{cL}^{JM\pi} \middle| V_{Cv} + V_{CC} \middle| \varphi_{c'L'}^{JM\pi} \right\rangle, \quad (16)$$

where the integration is performed over Ω_R and $\boldsymbol{r}$. The last term of Eq. (14) is nonlocal, and arises from the symmetrization operator P. The nonlocal potential $W_{cL,c'L'}^{J\pi}(R, R')$ can be

decomposed as

$$W^{J\pi}_{cL,c'L'}(R,R') = (E_c - E)\mathcal{N}^{J\pi}_{cL,c'L'}(R,R') + \mathcal{T}^{J\pi}_{cL,c'L'}(R,R') + \mathcal{V}^{J\pi}_{cL,c'L'}(R,R'), \quad (17)$$

which explicitly shows overlap $\mathcal{N}^{J\pi}_{cL,c'L'}$, kinetic energy $\mathcal{T}^{J\pi}_{cL,c'L'}$, and potential $\mathcal{V}^{J\pi}_{cL,c'L'}$ terms. The overlap kernel is defined from

$$\int \mathcal{N}^{J\pi}_{cL,c'L'}(R,R')g^{J\pi}_{c'L'}(R')dR' = R\left\langle \varphi^{JM\pi}_{cL} \middle| \varphi^{JM\pi}_{c'L'} \frac{g^{J\pi}_{c'L'}(R')}{R'} \right\rangle, \quad (18)$$

and equivalent expressions hold for the kinetic energy and potential kernels. Notice that similar terms shows up in the coupled-channel approach of transfer reactions [20]. We discuss the various contributions of Eq. (17) in the next subsection.

For scattering states ($E > 0$), a radial function $g^{J\pi}_{cL}(R)$ has the asymptotic behavior at large R values

$$g^{J\pi}_{cL,\omega L_\omega}(R) \to v_c{}^{-1/2} \times \left[I_L(k_cR)\delta_{c\omega}\delta_{LL_\omega} - U^{J\pi}_{cL,\omega L_\omega}O_L(k_cR)\right], \quad (19)$$

where ω is the entrance channel, I_L and O_L are the incoming and outgoing Coulomb functions, v_c and k_c are the velocity and wave number in channel c, and $\boldsymbol{U}^{J\pi}$ is the scattering matrix. In the R-matrix formalism [17], a channel radius a separates the internal region, where all terms of the potentials contribute, and the external region where only the monopole part of the Coulomb interaction is present. In the internal region, the radial wave function is expanded as

$$g^{J\pi}_{cL,\omega L_\omega}(R) = \sum_{i=1}^{N} f^{J\pi}_{cLi,\omega L_\omega}u_i(R), \quad (20)$$

where the N functions $u_i(R)$ represent the basis. The choice of the basis functions is discussed in Sec. II D.

B. Nonlocal terms

The nonlocal potential (17) arises from exchange effects due to the operator P [Eqs. (9) and (10)]. The overlap and potential kernels in Eq. (17) are obtained from

$$\begin{Bmatrix} \mathcal{N}^{J\pi}_{cL,c'L'}(R,R') \\ \mathcal{V}^{J\pi}_{cL,c'L'}(R,R') \end{Bmatrix} = \mathcal{J}RR' \iint \varphi^{JM\pi *}_{cL}(\Omega_R,\boldsymbol{r}) \times \begin{Bmatrix} 1 \\ V_{Cv}+V_{CC} \end{Bmatrix} \varphi^{JM\pi}_{c'L'}(\Omega_{R'},\boldsymbol{r}')d\Omega_R\, d\Omega_{R'}, \quad (21)$$

where

$$\mathcal{J} = \gamma^3 \quad (22)$$

is the Jacobian from coordinates $(\boldsymbol{r},\boldsymbol{R})$ to $(\boldsymbol{R},\boldsymbol{R}')$. Coordinates $(\boldsymbol{r},\boldsymbol{r}',\boldsymbol{R}_{CC})$ are expressed as

$$\boldsymbol{r} = -\gamma(\alpha\boldsymbol{R}+\boldsymbol{R}'),$$
$$\boldsymbol{r}' = -\gamma(\boldsymbol{R}+\alpha\boldsymbol{R}'),$$
$$\boldsymbol{R}_{CC} = \boldsymbol{r}-\boldsymbol{r}' = \frac{1}{\alpha+1}(\boldsymbol{R}-\boldsymbol{R}'). \quad (23)$$

In the case of a nucleon transfer, α is close to 1, and the relative coordinates $(\boldsymbol{r},\boldsymbol{r}')$ are large, even for relatively small values of $(\boldsymbol{R},\boldsymbol{R}')$. This means that the core-valence wave function needs to be accurately known up to large distances. If the binding energy is small, the nonlocal potentials are therefore very sensitive to the long-range part of the bound-state wave function.

The potential term is quite similar to the matrix elements involved in distorted wave Born approximation (DWBA) calculations [21], and its calculation is explained in several references (see, e.g., Refs. [21–23]). The calculation of the overlap and potential kernels is based on the expansions

$$\frac{u^{\ell j}_n(r)\,u^{\ell' j'}_{n'}(r')}{r^{\ell+1}r'^{\ell'+1}} = \sum_K N^K_{cc'}(R,R')P_K(\cos\theta_R),$$
$$\frac{u^{\ell j}_n(r)}{r^{\ell+1}}(V_{Cv}(r')+V_{CC}(R_{CC}))\frac{u^{\ell' j'}_{n'}(r')}{r'^{\ell'+1}} = \sum_K V^K_{cc'}(R,R')P_K(\cos\theta_R), \quad (24)$$

where θ_R is the angle between $\boldsymbol{R}$ and $\boldsymbol{R}'$, and $P_K(x)$ is a Legendre polynomial. The components $N^K_{cc'}(R,R')$ and $V^K_{cc'}(R,R')$ are obtained from numerical integrations. Notice that these expansions only depend on the quantum numbers of the projectile. They do not depend on the angular momenta J, L, L', and are therefore performed once.

The derivation of the kinetic-energy kernels is more tedious. However, we show in the Appendix, that they can be deduced from the overlap kernel as

$$\mathcal{T}^{J\pi}_{cL,c'L'}(R,R') = -\frac{\hbar^2}{2\mu}\left[\frac{\partial^2}{\partial R^2} - \frac{L(L+1)}{R^2}\right]\mathcal{N}^{J\pi}_{cL,c'L'}(R,R'). \quad (25)$$

The calculation of the nonlocal kernels from Eqs. (21) and (24) requires some angular-momentum algebra. We use the addition theorem

$$r^\ell Y^m_\ell(\Omega_r) = \sum_{\lambda=0}^{\ell} C^\lambda_\ell r_1^\lambda r_2^{\ell-\lambda}[Y_\lambda(\Omega_1)\otimes Y_{\ell-\lambda}(\Omega_2)]^{\ell m}, \quad (26)$$

where $\boldsymbol{r} = \boldsymbol{r}_1 + \boldsymbol{r}_2$ and

$$C^\lambda_\ell = \left[\frac{4\pi(2\ell+1)!}{(2\lambda+1)!(2\ell-2\lambda+1)!}\right]^{1/2}. \quad (27)$$

When the valence particle v has a spin zero, the overlap kernel can be expanded as

$$\mathcal{N}^{J\pi}_{cL,c'L'}(R,R') = \mathcal{J}(-\gamma)^{\ell+\ell'}\sum_K N^K_{c,c'}(R,R') \times \sum_{\lambda_1\lambda_2} C^{\lambda_1}_\ell C^{\lambda_2}_{\ell'}\alpha^{\lambda_1+\lambda_2}R^{\ell'+\lambda_1-\lambda_2+1}R'^{\ell-\lambda_1+\lambda_2+1} \times F^{J\pi}_{cL,c'L'}(K,\lambda_1,\lambda_2) \quad (28)$$

with

$$F^{J\pi}_{cL,c'L'}(K,\lambda_1,\lambda_2) = \left\langle \left[Y_L(\Omega_R)\otimes\left[Y_{\lambda_1}(\Omega_R)\otimes Y_{\ell-\lambda_1}(\Omega_{R'})\right]^{\ell}\right]^{JM} |P_K(\cos\theta_R)| \left[Y_{L'}(\Omega_{R'})\otimes\left[Y_{\ell'-\lambda_2}(\Omega_R)\otimes Y_{\lambda_2}(\Omega_{R'})\right]^{\ell'}\right]^{JM}\right\rangle. \quad (29)$$

The analytical calculation of these coefficients requires some algebra to modify the order of angular-momentum couplings, and involves $6j$ coefficients. When the valence particle has a spin, further angular-momentum recoupling is necessary. A simple value is obtained for $\ell = \ell' = 0$, where we have

$$F^{J\pi}(K,0,0) = \frac{\delta_{KJ}}{4\pi(2J+1)}. \quad (30)$$

C. Symmetry of the nonlocal kernels

Let us briefly discuss the symmetry properties of the nonlocal potential (17). According to Eq. (9), we have, when the cores are bosons,

$$P\Psi^{JM\pi} = \Psi^{JM\pi}, \quad (31)$$

which means that the property

$$[H,P] = 0 \quad (32)$$

should be satisfied. This implies that both V_{Cv} potentials in Eqs. (1) and (12) are identical. For example, in the $^{13}C+^{12}C$ system, the $n+^{12}C$ (real) potential associated with the ^{13}C ground state should be identical to the $n+^{12}C$ optical potential which describes the neutron-target scattering. If this condition is fulfilled, the nonlocal potential $W^{J\pi}$ is symmetric, and we have

$$W^{J\pi}_{cL,c'L'}(R,R') = W^{J\pi}_{c'L',cL}(R',R). \quad (33)$$

This test is very strong since, individually, all terms of the right-hand side of Eq. (17) are not symmetric. In practical applications, however, it may seem more physical to choose different potentials: one which binds the $C+v$ system, and the other which is adapted to the $C+v$ scattering. In such a case, the symmetry property (33) is approximately satisfied (see the discussion in Ref. [14]). This means that some properties of the scattering matrix, such as the symmetry or the unitarity (for real potentials), are not any more valid. We choose to restore the symmetry of the nonlocal potential through

$$W^{J\pi}_{cL,c'L'}(R,R') \to \tfrac{1}{2}\left[W^{J\pi}_{cL,c'L'}(R,R') + W^{J\pi}_{c'L',cL}(R',R)\right]. \quad (34)$$

We will see in some examples that these effects, in practice, are small. The main reason is that, in general, the contribution of the optical potential V_{Cv} is small compared to the optical potential between the cores.

D. Elastic cross sections

The elastic cross sections are obtained from the scattering matrices $\boldsymbol{U}^{J\pi}$ [see Eq. (19)]. According to the scattering theory, the elastic cross section between different particles is defined from the scattering amplitude as

$$\frac{d\sigma}{d\theta} = |f(\theta)|^2,$$
$$f(\theta) = f^{\rm N}(\theta) + f^{\rm C}(\theta), \quad (35)$$

where θ is the scattering angle. In this definition, $f^{\rm C}(\theta)$ is the Coulomb amplitude and $f^{\rm N}(\theta)$ is the nuclear amplitude, defined by

$$f^{\rm N}(\theta) = \frac{1}{2ik}\sum_J (2J+1)P_J(\cos\theta)(U^J-1)e^{2i\sigma_J}, \quad (36)$$

where σ_J is the Coulomb phase shift. For the sake of simplicity, we consider single-channel systems with spin 0 nuclei. The generalization is straightforward (see, for example, Ref. [21]).

As explained in Sec. II A, the scattering matrices are obtained from the resolution of a Schrödinger equation involving a nonlocal potential. Let us denote as U^J_0 and $g^J_0(R)$ the scattering matrix and wave function obtained from the local term (16) only. These quantities are obtained without symmetrization of the wave function (9). The integral definition of the scattering matrix [24] provides a relationship between U^J and U^J_0 as

$$U^J = U^J_0 + U^J_{\rm ex},$$
$$U^J_{\rm ex} = -\frac{i}{\hbar}\iint g^J_0(R)W^J(R,R')g^J(R')dRdR'. \quad (37)$$

Consequently the nuclear scattering amplitude can be written as

$$f^{\rm N}(\theta) = f^{\rm N}_0(\theta) + f^{\rm N}_{\rm ex}(\theta), \quad (38)$$

where $f^{\rm N}_0(\theta)$ is obtained from Eq. (36) with the scattering matrices U^J_0, and where the exchange amplitude $f^{\rm N}_{\rm ex}(\theta)$ is the nonlocal contribution

$$f^{\rm N}_{\rm ex}(\theta) = \frac{1}{2ik}\sum_J (2J+1)P_J(\cos\theta)U^J_{\rm ex}e^{2i\sigma_J}. \quad (39)$$

A similar decomposition has been suggested in Refs. [25–27]. Since the calculation of the exchange amplitude $f^{\rm N}_{\rm ex}(\theta)$ is based on a nonlocal potential, it is common in the literature to assume that it can be simulated by the transfer of the valence particle (see for example Ref. [27], and references therein). In other words, the exchange amplitude can be approximated as

$$f^{\rm N}_{\rm ex}(\theta) \approx f_{\rm tr}(\pi-\theta), \quad (40)$$

where $f_{\rm tr}(\pi-\theta)$ is the transfer amplitude, usually computed at the DWBA approximation [22]. In this approximation, however, the exact wave function $g^J(R)$ is replaced by the nonsymmetrized wave function $g^J_0(R)$ in Eq. (37), and the nonlocal potential $W^J(R,R')$ is approximated from an auxiliary potential.

Another difference is related to the spectroscopic factors. As expected in transfer calculations, the DWBA amplitude $f_{\rm tr}(\pi-\theta)$ is multiplied by the spectroscopic factor of the projectile. This multiplicative factor, however, does not show up in the present approach. The two-body wave function (6) is of course an approximation which can be improved, either by introducing a spectroscopic factor or by including core excitations. The introduction of a spectroscopic factor in Eq. (6), however, represents a global renormalization of the expansion (7), and therefore of the symmetrized definition (9). The scattering matrices deduced from Eq. (19) are therefore

not affected by a spectroscopic factor. Introducing core excitations in the present approach is a challenge for future works, but is beyond the scope of the present work.

E. Lagrange functions

As mentioned before, the scattering matrices are calculated with the R-matrix method, which is based on a channel radius a and on the choice of basis functions u_i. As in previous works, we choose Lagrange functions which permit fast and accurate calculations of the matrix elements, in particular for nonlocal potentials (see Ref. [18] for detail).

The calculation of the R matrix is based on matrix elements between basis functions over the internal region. The main input is the matrix defined from

$$C^{J\pi}_{cLi,c'L'j} = \langle u_i|(T_R + E_c - E)\delta_{cc'}\delta_{LL'} + V^{J\pi}_{cL,c'L'} + W^{J\pi}_{cL,c'L'}|u_j\rangle. \quad (41)$$

For example, matrix elements of the local and nonlocal potentials are given by

$$\langle u_i|V|u_j\rangle = \int_0^a u_i(R)V(R)u_j(R)\,dR,$$
$$\langle u_i|W|u_j\rangle = \int_0^a\int_0^a u_i(R)W(R,R')u_j(R')\,dRdR'. \quad (42)$$

These calculations are greatly simplified by using N Lagrange functions for u_i which are defined by

$$u_i(R) = (-1)^{N+i}\frac{R}{R_i}\sqrt{R_i\left(1-\frac{R_i}{a}\right)}\frac{P_N(2R/a-1)}{R-R_i}, \quad (43)$$

where R_i are the zeros of

$$P_N(2R/a-1) = 0. \quad (44)$$

The normalization of Eq. (43) is chosen in such a way that the Lagrange condition

$$u_i(R_j) = \frac{1}{\sqrt{a\lambda_i}}\delta_{ij} \quad (45)$$

is satisfied. In this equation, λ_i is the weight of the Gauss-Legendre quadrature associated with the [0,1] interval.

With the choice of basis function (43), the calculation of the matrix elements (42) is extremely simple if the Gauss approximation of order N is used for the quadratures. At this approximation, the matrix elements are given by

$$\langle u_i|V|u_j\rangle \approx V(R_i)\delta_{ij},$$
$$\langle u_i|W|u_j\rangle \approx a\sqrt{\lambda_i\lambda_j}W(R_i,R_j), \quad (46)$$

and no numerical integral is required for the matrix elements. We refer to Refs. [17,18] for details.

III. APPLICATIONS

A. The $^{13}C + ^{12}C$ system

The $^{13}C + ^{12}C$ system has been intensively studied experimentally [28,29] as well as theoretically [13,14,30]. It is known that nonlocal effects can be simulated by a parity-dependent optical potential [15]. Owing to the one-neutron exchange, the potentials for even and odd partial waves are different [31]. In the "extreme" situation of identical nuclei, odd partial waves are strictly forbidden.

We have determined the nonlocal potential (17) from $^{12}C + ^{12}C$ and $n + ^{12}C$ potentials. For $^{12}C + ^{12}C$, we take the optical potential derived by Treu *et al.* [32], and defined (in MeV) as

$$V_{CC}(r) = -\frac{100}{1+\exp[(r-5.45)/0.48]} - i\frac{15}{1+\exp[(r-5.77)/0.26]}, \quad (47)$$

where r is expressed in fm. A Coulomb point-sphere potential of radius $R_C = 5.45$ fm is added. This optical potential is fitted on elastic-scattering data around the Coulomb barrier. In all applications, we use the integer masses with $\hbar^2/2m_N = 20.736$ MeV fm^2 (m_N is the nucleon mass).

The $n + ^{12}C$ potential is chosen as in Ref. [33], i.e.,

$$V_{nC}(\boldsymbol{r}) = -\frac{V_0}{1+\exp[(r-r_0)/a_0]} - (\boldsymbol{\ell}\cdot\boldsymbol{s})\frac{V_{\ell s}}{r}\frac{d}{dr}\frac{1}{1+\exp[(r-r_0)/a_0]}, \quad (48)$$

where $V_0 = 62.70$ MeV for ℓ even and 50.59 MeV for ℓ odd, and where $r_0 = 2.656$ fm and $a_0 = 0.705$ fm. The spin-orbit amplitude is $V_{\ell s} = 28.406$ MeV. This potential reproduces the experimental energies of the first $1/2^-$, $1/2^+$, and $5/2^+$ states in ^{13}C. Between the target and the projectile, the same $n + ^{12}C$ potential is adopted for each partial wave, corresponding to the central part of Eq. (48). Once potentials (47) and (48) are determined, the model does not contain any free parameter.

In Fig. 2, the $^{13}C + ^{12}C$ elastic cross sections at $E_{c.m.} = 7.8$ and 14.2 MeV are shown. In each case, we consider four conditions: (1) when only the local potential is included, the backward angle enhancement of the cross section is not reproduced; (2) the nonlocal calculation involving the ^{13}C ground state only (dashed line) reproduces fairly well the data; (3) when the $1/2^+$ and $5/2^+$ excited states are introduced (solid line), elastic scattering is not significantly modified; (4) in the $n + ^{12}C$ potential between the target and the projectile (dotted line), we have replaced the real potential (48) by the Koning-Delaroche parametrization [34]. Although some symmetry properties are lost (see Sec. II B), there is a weak influence on the $^{13}C + ^{12}C$ cross section.

Figure 2(c) presents the amplitudes $|U^{J\pi}_L|$ of the scattering matrices (elastic channel) at $E_{c.m.} = 7.8$ MeV. We choose here $J = L - 1/2$ but a similar behavior is observed for $J = L + 1/2$. Without the nonlocal part of the potential, the variation is smooth. As expected, the nonlocality leads to a splitting between odd and even L values. This property gives rise to the backward angle enhancement of the cross section, and justifies the use of parity-dependent optical potentials [15] to simulate non-local effects. An advantage of the present method is that it does not require any additional parameter. In addition, excited states of the $n + ^{12}C$ system are included in a straightforward way.

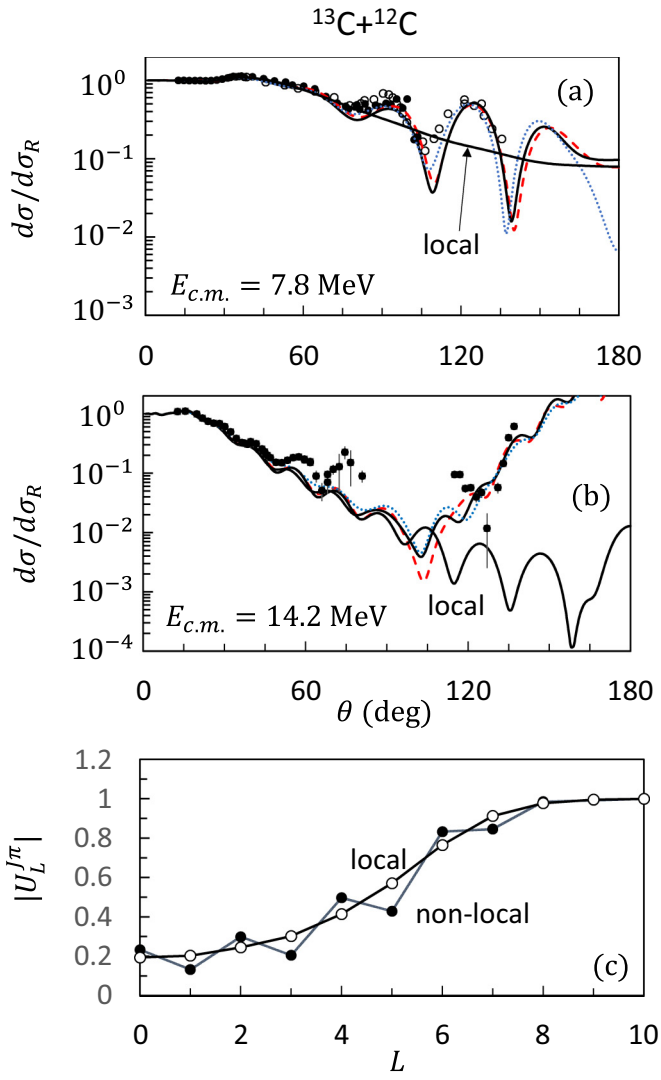

FIG. 2. ^{13}C + ^{12}C elastic cross sections (divided by the Rutherford cross section) at $E_{\text{c.m.}} = 7.8$ MeV (a) and 14.2 MeV (b). The data are taken from Refs. [28] (full dots) and [29] (open dots). The solid lines are obtained with the $1/2^-, 1/2^+, 5/2^+$ states of ^{13}C. The dashed (red) lines correspond to the $1/2^-$ ground state only. The dotted (blue) lines are obtained with different $n + ^{12}$C potentials in the entrance and exit channels (see text). (c) presents the amplitudes $|U_L^{J\pi}|$ of the scattering matrices at $E_{\text{c.m.}} = 7.8$ MeV, and for $J = L - 1/2$.

In Fig. 3, we investigate the inelastic cross sections to the ^{13}C($1/2^+$) and ^{13}C($5/2^+$) states, which have been measured in Ref. [35] at energies around the Coulomb barrier. The effect of the nonlocality is quite important. With the local potential only, the theoretical cross sections are far below the data. The calculation involves the ^{13}C(gs, $1/2^+, 5/2^+$) + ^{12}C channels. Here the cross sections are more sensitive to the choice of the $n + ^{12}$C potential. Let us emphasize that there is no fit of the cross sections. All inputs are kept identical as for elastic scattering.

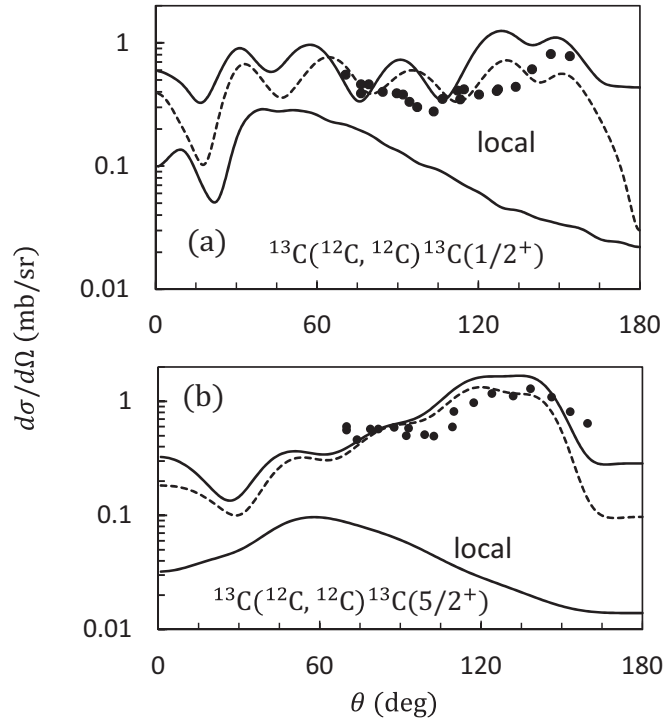

FIG. 3. Inelastic ^{13}C + ^{12}C cross sections to the $1/2^+$ (a) and $5/2^+$ (b) states of ^{13}C at $E_{\text{c.m.}} = 9.88$ MeV. The experimental data are taken from Ref. [35]. Solid (dashed) lines are obtained with identical (different) $n + ^{12}$C potentials in the entrance and exit channels (see text).

B. The ^{13}N + ^{12}C system

With the development of radioactive beams, the ^{13}N + ^{12}C mirror system has attracted much attention in the literature [28,30]. Measurements have provided some information about charge-symmetry and about the parity effect [28]. Figure 4 shows the ^{13}N + ^{12}C calculated cross sections. Only the ^{13}N ground state is bound, and has been introduced in the calculation. With respect to the ^{13}C + ^{12}C system, the only difference is the introduction of a Coulomb term for $p + ^{12}$C (with $R_C = 2.7$ fm). The binding energy of ^{13}N is -1.90 MeV, in fair agreement with experiment (-1.94 MeV). Here again the model reproduces remarkably well the experimental data [28].

C. The ^{16}O + ^{12}C system

In the ^{16}O + ^{12}C scattering, an α particle is exchanged between the target and the projectile. This system has been intensively investigated in the literature (see, for example, Refs. [25–27] for recent works).

We consider the elastic-scattering data of Villari *et al.* [36] at the typical energy $E_{\text{c.m.}} = 23.14$ MeV, where a backward-angle enhancement of the cross sections is observed. We use the same ^{12}C + ^{12}C core-core potential (47) as in previous applications. For the $\alpha + ^{12}$C system, we adopt the potentials used in Ref. [37], i.e., a Woods-Saxon potential with a range $R_0 = 4.15$ fm and a diffuseness $a = 0.55$ fm. In addition to the 0^+ ground state, we include the 1^-, 3^-, and 2^+ excited states. Since the 2^+ state presents a cluster structure, R_0 is chosen

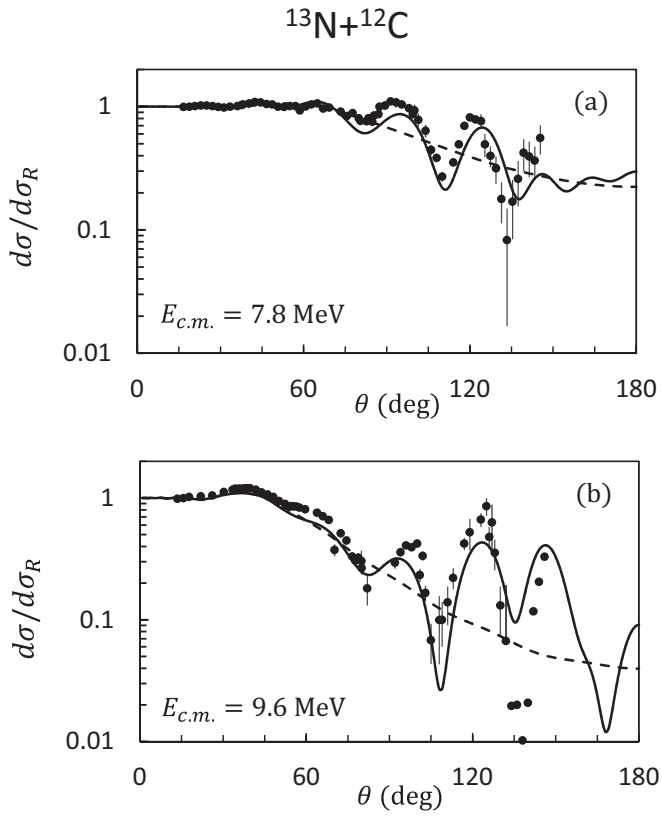

FIG. 4. $^{13}\mathrm{N}+^{12}\mathrm{C}$ elastic cross sections (divided by the Rutherford cross section) at $E_{\mathrm{c.m.}} = 7.8$ MeV (a) and 9.6 MeV (b). The data are taken from Ref. [28]. Solid lines correspond to the full calculation, and dashed lines to the local potential only.

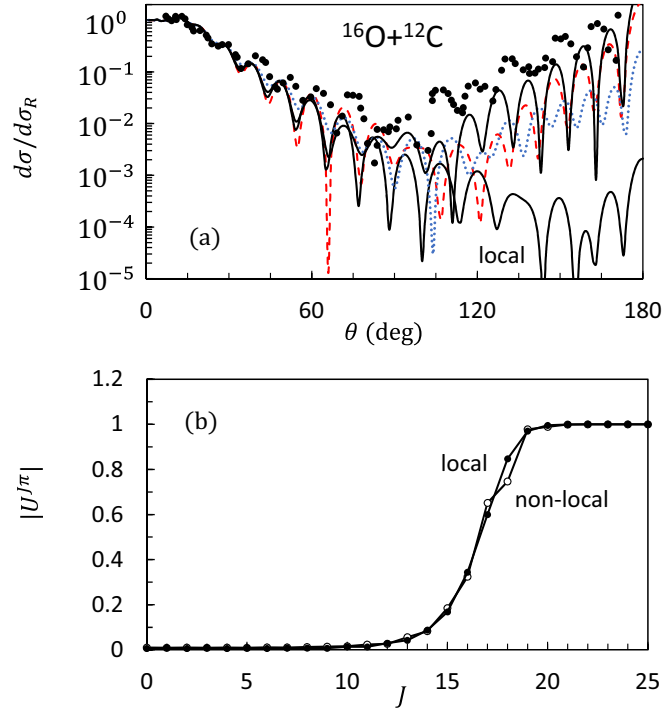

FIG. 5. $^{16}\mathrm{O}+^{12}\mathrm{C}$ elastic cross section (divided by the Rutherford cross section) at $E_{\mathrm{c.m.}} = 23.14$ MeV (a). The data are taken from Ref. [36]. The solid lines correspond to the multichannel model. The dashed lines are obtained with the ^{16}O ground state only, and the dotted lines with different $\alpha + ^{12}$C potentials (see text). Panel (b) presents the amplitudes $|U^{J\pi}|$ of the scattering matrices.

larger (4.5 fm) for this state. The Coulomb potential has a point-sphere shape with a radius $R_C = 4.15$ fm. The depths of the potentials V_0 are adjusted to the experimental binding energies, which provides $V_0 = -43.25, -68.95, -41.3$, and -42.4 MeV for the $0^+, 2^+, 1^-$, and 3^- states, respectively. Between the target and the projectile, the same $\alpha + ^{12}$C potential is adopted, corresponding to the ^{16}O ground state.

The elastic cross section is presented in Fig. 5(a) in different conditions. The calculation with the local potential provides a fair description of the data up to $\theta \approx 90^\circ$, but does not reproduce the enhancement at large angles. With the nonlocal term, even if the oscillations at backward angles are not exactly reproduced, the role of inelastic channels is obvious. The present model, based on the exchange of an α particle during the collision, cannot be expected to be perfect. Other channels are open, such as the neutron or proton transfer, but are neglected here. There are usually treated by phenomenological potentials involving additional parameters.

In the $^{16}\mathrm{O}+^{12}\mathrm{C}$ system, the role of the core-valence potential in more important than in $^{13}\mathrm{C}+^{12}\mathrm{C}$. To assess this sensitivity, we have also used the α optical potential of Avrigeanu *et al.* [38] [dotted line in Fig. 5(a)]. This is explained by the long range of the $\alpha + ^{12}$C potential, due to the Coulomb term. In this system, using a consistent $\alpha + ^{12}$C potential in the entrance and in the exit channels seems more appropriate.

The amplitude of the scattering matrices $|U^{J\pi}|$ is displayed in Fig. 5(b). As for $^{13}\mathrm{C}+^{12}\mathrm{C}$, the calculation with the non-local term provides differences between even and odd partial waves. These differences, however, are weaker than in $^{13}\mathrm{C}+^{12}\mathrm{C}$. As observed in Ref. [27], the even-odd effect is stronger around the grazing angular momentum ($J \approx 18$).

IV. DISCUSSION OF THE NONLOCALITY

A. Local equivalent potentials

The effects of the nonlocality can be simulated by an equivalent local potential. For the sake of simplicity, we assume a single-channel problem. The extension to multichannel systems is simple and does not modify the conclusions. In a single-channel model, the radial Schrödinger equation reads

$$\left[-\frac{\hbar^2}{2\mu}\left(\frac{d^2}{dr^2} - \frac{L(L+1)}{R^2}\right) + V^{J\pi}(R) - E\right] g^{J\pi}(R) + \int W^{J\pi}(R,R')g^{J\pi}(R')dR' = 0 \tag{49}$$

and can be replaced by

$$\left[-\frac{\hbar^2}{2\mu}\left(\frac{d^2}{dr^2} - \frac{L(L+1)}{R^2}\right) + V^{J\pi}_{\mathrm{eq}}(R) - E\right] g^{J\pi}(R) = 0, \tag{50}$$

where the equivalent potential $V^{J\pi}_{\rm eq}(R)$ is given by

$$V^{J\pi}_{\rm eq}(R) = V^{J\pi}(R) + \frac{1}{g^{J\pi}(R)} \int W^{J\pi}(R,R')g^{J\pi}(R')dR'. \tag{51}$$

This potential depends on the angular momentum, and presents singularities at the nodes of the wave functions. Thompson *et al.* [39] have proposed to define a smooth, J-independent, effective potential by

$$V^{\pi}_{\rm eff}(R) = \frac{\sum_J \omega^{J\pi}(R) V^{J\pi}_{\rm eq}(R)}{\sum_J \omega^{J\pi}(R)}, \tag{52}$$

where the weight factors $\omega^{J\pi}(R)$ are given by

$$\omega^{J\pi}(R) = (2J+1)(1-|U^{J\pi}|^2)|g^{J\pi}(R)|^2. \tag{53}$$

In this way, the influence of the nodes is reduced and the potential (53) does not depend on J. However, the scattering matrices obtained with Eq. (52) are not strictly identical to those obtained with Eq. (49) or (50). A test with the cross sections must be performed to check the accuracy of the potential (52).

As we expect the equivalent local potentials to depend on parity, the potential (52) is defined for each parity. From $V^{+}_{\rm eff}(R)$ and $V^{-}_{\rm eff}(R)$, we determine central and parity-dependent potentials as

$$\begin{aligned} V_0(R) &= \tfrac{1}{2}(V^{+}_{\rm eff}(R) + V^{-}_{\rm eff}(R)), \\ V_\pi(R) &= \tfrac{1}{2}(V^{+}_{\rm eff}(R) - V^{-}_{\rm eff}(R)). \end{aligned} \tag{54}$$

The present work, based on rigorous non-local potentials, offers the possibility to investigate the parity potential which, in general, is phenomenological (see, for example, Ref. [28]). Notice that both $V_0(R)$ an $V_\pi(R)$ contain real and imaginary components. A parity effect can be also deduced from techniques based on data inversion [27,40].

B. Asymptotic form of the nonlocal kernels

Here, we present some qualitative aspects regarding the nonlocal kernels, and in particular the overlap kernel $\mathcal{N}^{J\pi}_{cL,c'L'}(R,R')$. Let us first discuss the overlap functions $N^{K}_{cc'}(R,R')$ which show up in Eq. (24). To simplify the presentation, we assume that the valence particle is a neutron in a s state. In that case, the core-valence wave function tends to

$$u_0(r) \to C\exp(-k_B r), \tag{55}$$

where k_B is the wave number and C the asymptotic normalization coefficient (ANC).

To develop further, we use the expansion [15]

$$\frac{\exp(-k|\boldsymbol{r}_1-\boldsymbol{r}_2|)}{k|\boldsymbol{r}_1-\boldsymbol{r}_2|} = \frac{2}{\pi}\sum_\ell (2\ell+1) i_\ell(kr_<)k_\ell(kr_>)P_\ell(\cos\theta_r), \tag{56}$$

where $r_< = \min(r_1,r_2)$ and $r_> = \max(r_1,r_2)$, and where θ_r is the angle between $\boldsymbol{r}_1$ and $\boldsymbol{r}_2$. In this definition, $i_\ell(x)$ and $k_\ell(x)$ are modified spherical Bessel functions [41]. For large arguments, they tend to

$$\begin{aligned} i_\ell(x) &\to \frac{\exp(x)}{2x}, \\ k_\ell(x) &\to \pi\frac{\exp(-x)}{2x}. \end{aligned} \tag{57}$$

Using the expansion (56) for $u_0(r)$ and $u_0(r')$, and using relations (23), we find, for large (R,R') values,

$$\frac{u_0(r)u_0(r')}{rr'} \to \sum_K N^{K,\rm as}(R,R')P_K(\cos\theta_R). \tag{58}$$

In the range $\alpha R' < R < R'/\alpha$, the asymptotic kernels are defined by

$$\begin{aligned} N^{K,\rm as}(R,R') = \frac{4}{\pi^2}k_B^2 C^2(-1)^K \sum_{\ell_1\ell_2}(2\ell_1+1)(2\ell_2+1) \\ \times \langle \ell_1 0 \ell_2 0|K0\rangle^2 k_{\ell_2}(\gamma k_B R)k_{\ell_1}(\gamma k_B R') \\ \times i_{\ell_1}(\alpha\gamma k_B R)i_{\ell_2}(\alpha\gamma k_B R'), \end{aligned} \tag{59}$$

and Eq. (57) provides

$$N^{K,\rm as}(R,R') \sim \frac{1}{R^2R'^2}\exp\left(-\frac{k_B}{1+\alpha}(R+R')\right). \tag{60}$$

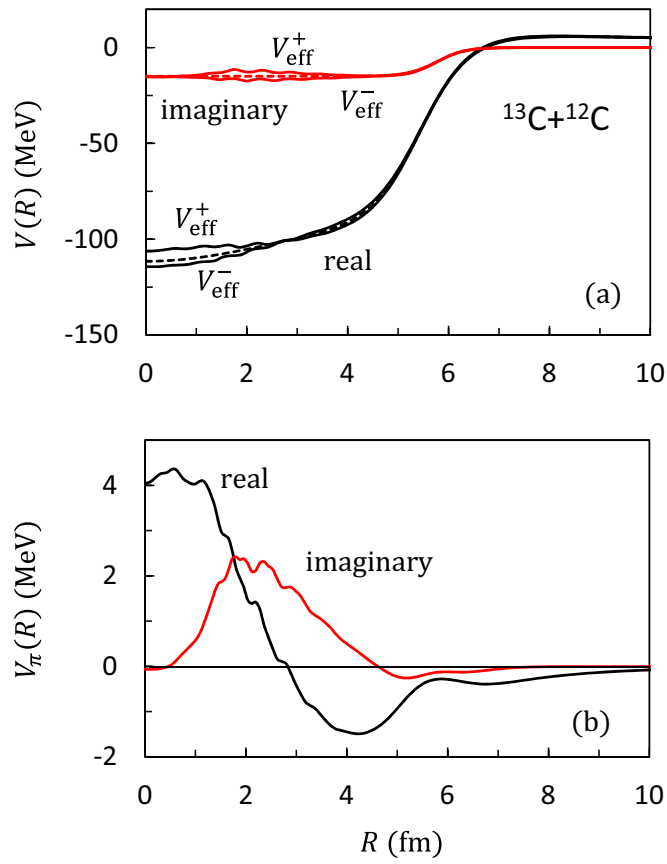

FIG. 6. Local effective potentials for the ^{13}C + ^{12}C system at $E_{\rm c.m.} = 7.8$ MeV. In (a), the dashed curve corresponds to the local potential, and the solid curves to the local equivalent potentials (52). (b) displays the parity potential $V_\pi(R)$ [Eq. (54)].

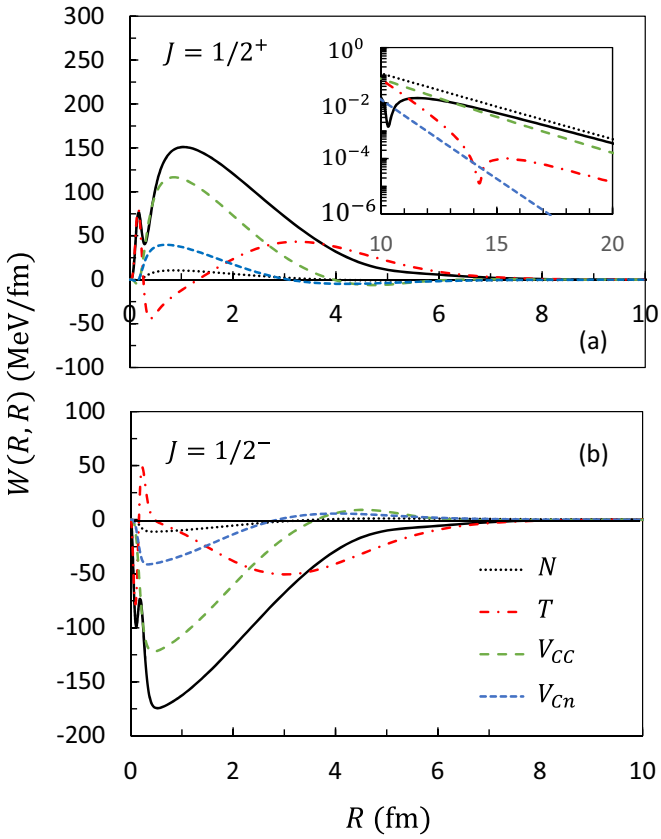

FIG. 7. Contributions of the overlap, kinetic energy, and potentials (V_{CC} and V_{Cn}) to the nonlocal kernel (17) for $R = R'$, and for $J = 1/2^+$ (a) and $J = 1/2^-$ (b) in the $^{13}C + ^{12}C$ system ($E_{c.m.} = 7.8$ MeV). The overlap kernel is multiplied by $-E_{c.m.}$. For V_{CC}, the real part is displayed. The inset focuses on the long-range part in a logarithmic scale.

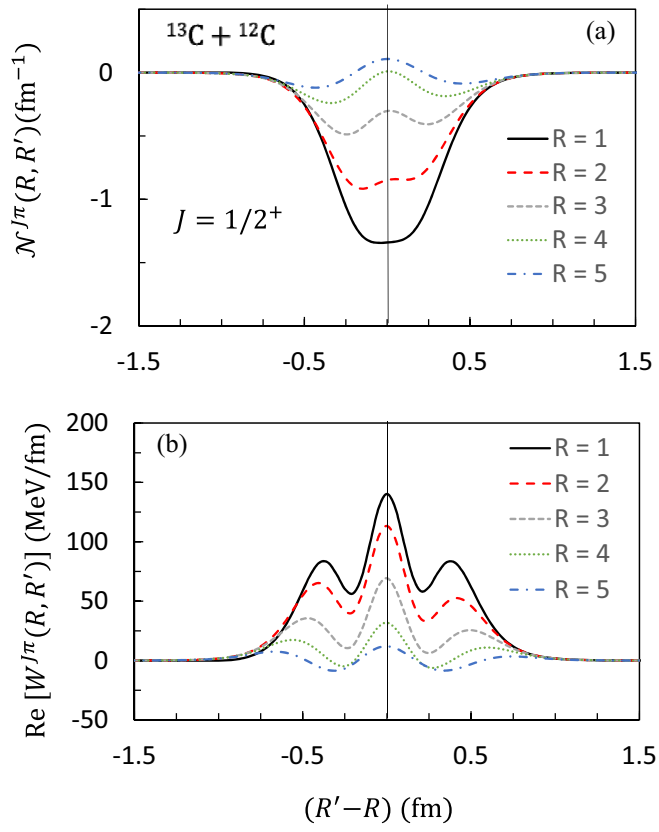

FIG. 8. Nonlocal kernels $\mathcal{N}(R,R')$ (a) and $W(R,R')$ [real part, (b)] for the $^{13}C + ^{12}C$ system ($J = 1/2^+$), as a function of $(R' - R)$ [see Eq. (17)]. The curves are plotted for different R values.

As α is in general close to 1, Eqs. (59) and (60) are valid for $R \approx R'$. Otherwise, a similar development gives

$$N^{K,\mathrm{as}}(R,R') \sim \frac{1}{R^2 R'^2} \exp\left(-\frac{k_B}{1-\alpha}|R-R'|\right). \tag{61}$$

This shows that the nonlocality overlap kernel presents an exponential decrease, associated with the binding energy of the projectile.

When the angular momentum is not an s wave, the expansion (56) can be generalized [15], but this does not change the general trend. In addition, if the transferred particle is charged, the asymptotic behavior takes the form

$$u_0(r) \to C\frac{\exp(-k_B r)}{r^{\eta_B}}, \tag{62}$$

where η_B is the Sommerfeld parameter. The faster decrease can be simulated by using Eq. (55) with a (larger) effective wave number, which simulates Coulomb effects [42]. Consequently, Eq. (59) remains qualitatively valid, even for charged transferred particles.

The nonlocal potentials (17) also involve kinetic-energy and nucleus-nucleus potential terms. As discussed in Sec. II B, the kinetic-energy kernel is directly deduced from a second derivative of the overlap. The asymptotic behaviour is therefore similar to Eq. (59). To determine the potential contribution, we start from definition (24). The first term in the potential $V_{Cv}(r')$ is involved in standard DWBA calculations (post form) [21]. For a transferred neutron, the nuclear contribution in V_{Cv} makes this term short-ranged. The asymptotic behavior (60) is therefore modified, with a smaller range. In contrast, the core-core interaction V_{CC} always presents a Coulomb term. One therefore expects this interaction to be dominant at large distances.

The non-local potentials in Eq. (17) are obtained from Eqs. (24) and (55), and from angular matrix elements [21,23]. The procedure is similar to the one followed in DWBA calculations. If the internal angular momenta are taken as $\ell = \ell' = 0$, the calculation is simple, as the sum over K contains a single term $K = J$. We have

$$\begin{aligned}\mathcal{N}^{J\pi}(R,R') &= \mathcal{J}RR'N^J(R,R')/(2J+1),\\ \mathcal{V}^{J\pi}(R,R') &= \mathcal{J}RR'\big(V^J_{Cv}(R,R') + V^J_{CC}(R,R')\big)/(2J+1).\end{aligned} \tag{63}$$

Equation (59) contains a phase factor $(-1)^J$ at large distances, which shows that the nonlocal potentials have opposite signs for even and odd partial waves. This effect arises from the symmetrization of the wave functions for the core exchange. As shown by von Oertzen [13], it can be simulated by a local, parity-dependent, potential. An application to the

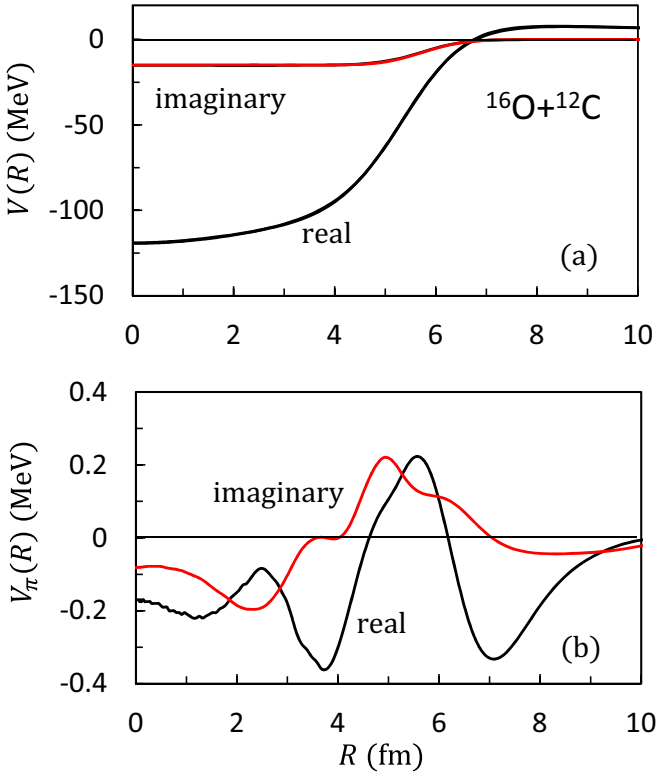

FIG. 9. Local effective potentials for the $^{16}\mathrm{O}+^{12}\mathrm{C}$ system at $E_{\mathrm{c.m.}} = 23.14$ MeV. In (a), the local potential and the equivalent potential (52) are superimposed. (b) displays the parity potential $V_\pi(R)$ [Eq. (54)].

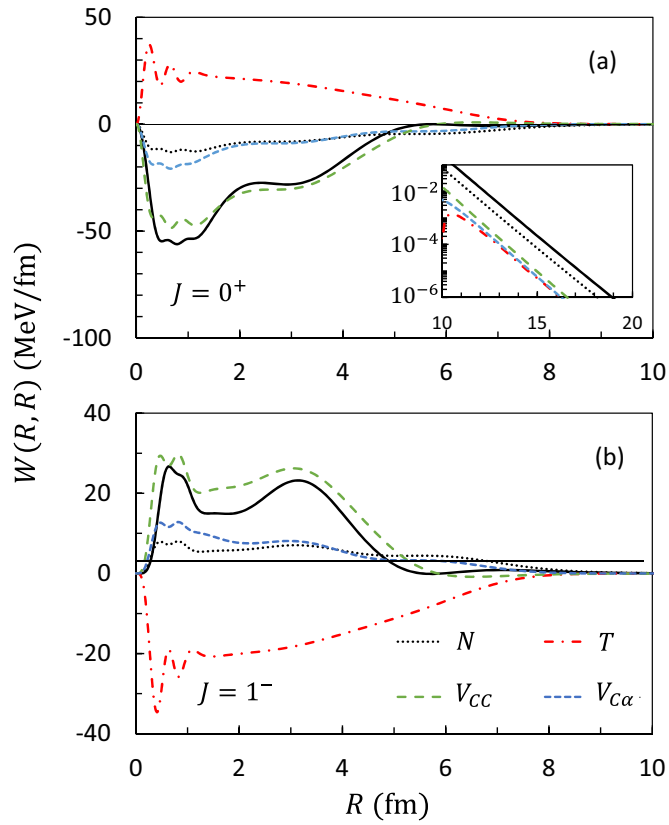

FIG. 10. Contributions of the overlap, kinetic energy and potential (V_{CC} and $V_{C\alpha}$) to the nonlocal kernel (17) for $R = R'$, and for $J = 0^+$ (a) and $J = 1^-$ (b) in the $^{16}\mathrm{O}+^{12}\mathrm{C}$ system. The real part of V_{CC} is shown. The inset focuses on the long-range part in a logarithmic scale.

analysis of the $^{13}\mathrm{C}+^{12}\mathrm{C}$ and of the $^{13}\mathrm{N}+^{12}\mathrm{C}$ systems can be found in Ref. [28].

C. Application to $^{13}\mathrm{C}+^{12}\mathrm{C}$

In Fig. 6, we present the effective potentials for the $^{13}\mathrm{C}+^{12}\mathrm{C}$ system at $E_{\mathrm{c.m.}} = 7.8$ MeV. For the sake of simplicity, we discuss the single-channel calculation. Figure 6(a) shows the local potential (dashed lines), and the parity-dependent effective potentials (solid lines) obtained with Eq. (54). The elastic cross sections obtained with this effective potential is very close to the original cross section (they are almost indistinguishable in a figure). As expected, the potentials present small oscillations due to the nodes in the scattering wave functions. We have repeated the calculations with different numerical conditions (channel radius, number of basis functions), and checked that the effective potentials are quite stable. Figure 6(b) display the parity potential V_π [see Eq. (54)]. The parity effect is important in the real part as well as in the imaginary part.

In Fig. 7, we display the different contributions in the nonlocal kernel $W^{J\pi}(R,R')$ Eq. (17) for $R = R'$ at $E_{\mathrm{c.m.}} = 7.8$ MeV. Four terms are present: the overlap, the kinetic energy, and two contributions of the potential (the core-core and core-valence terms). Partial waves $J = 1/2^+$ $(L = 1)$ and $J = 1/2^-$ $(L = 0)$ are shown in panels (a) and (b). The change of sign between both parities is confirmed. At short distances, the main contribution comes from V_{CC}, but the kinetic-energy term is dominant at large distances. For consistency, the overlap is multiplied by $-E_{\mathrm{c.m.}}$, and represents a small contribution. The inset of panel (a) confirms the asymptotic behavior. All terms but V_{Cv} have the same exponential behavior. The contribution associated with V_{Cv} presents a faster decrease owing to the absence of the Coulomb interaction.

In Fig. 8, we analyze the nonlocality for $R \neq R'$ and for $J = 1/2^+$. We plot the overlap and real-potential kernels as a function of $(R' - R)$ for various R values. For small R values, the shape of the overlap kernel is close to a Gaussian, which justifies the Perey-Buck approximation [43]. However, for $R > 1$ fm, the shape is more complicated than a Gaussian factor. As expected the main effect of the nonlocality comes from $|R - R'| \lesssim 1$ fm.

D. Application to $^{16}\mathrm{O}+^{12}\mathrm{C}$

The local effective potentials (52) for $^{16}\mathrm{O}+^{12}\mathrm{C}$ at $E_{\mathrm{c.m.}} = 23.14$ MeV are presented in Fig. 9(a). Again, we limit the discussion to the single-channel system. Since the depth of these potentials is rather large, the differences with the exact local potential (16) are small, indistinguishable at the scale of the figure. Figure 9(b) shows the parity potential (54).

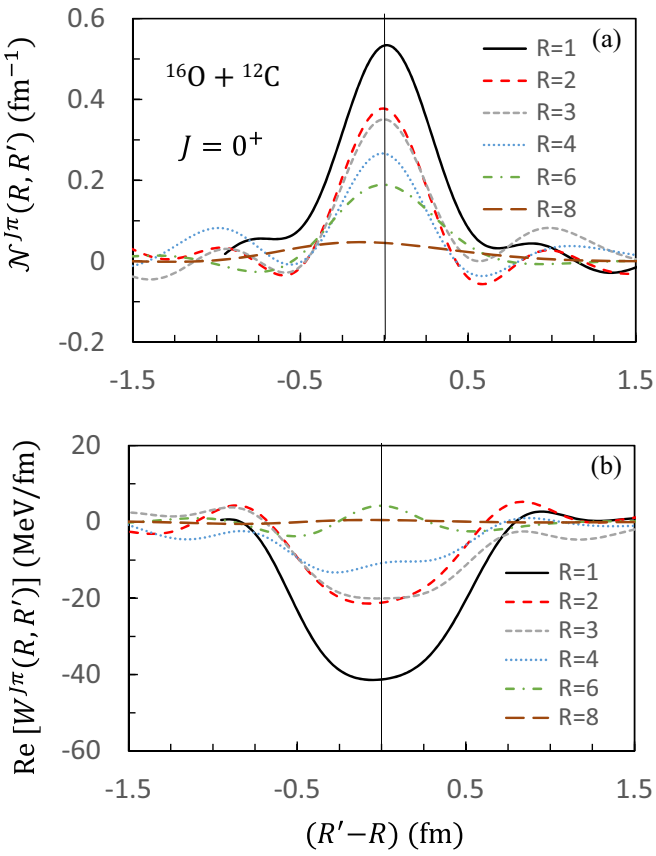

FIG. 11. Nonlocal kernels $\mathcal{N}(R,R')$ (a) and $W(R,R')$ [real part, (b)] for the $^{16}O + ^{12}C$ system ($J = 0^+$), as a function of $(R' - R)$ [see Eq. (17)]. The curves are plotted for different R values.

As for $^{13}C + ^{12}C$, these potentials present oscillations due to the nodes of the scattering wave functions. Although the amplitude is small, the effect of the parity potential extends to large distances. This explains that this potential provides a large backward-angle enhancement of the cross section (see Fig. 5). The cross sections provided by the effective potential (52) are very close to the original cross sections of Fig. 5.

The decomposition of the nonlocal kernel (17) in different terms is presented in Fig. 10 for $J = 0^+$ (a) and $J = 1^-$ (b). The dominant contribution comes from the core-core potential V_{CC}. There is a cancellation effect of the overlap, kinetic-energy, and $V_{C\alpha}$ contributions. At large distances the decrease of the potentials [inset of Fig. 10(a)] is much faster than in $^{13}C + ^{12}C$ (see Fig. 7). This is explained by Eq. (60) since k_B is much larger in ^{16}O than in ^{13}C (and coefficient α is smaller).

The nonlocality for $R \neq R'$ is illustrated in Fig. 11 for $J = 0^+$. As for $^{13}C + ^{12}C$, the shape of the overlap kernel is close to a Gaussian for small R values, but deviates when R increases.

V. CONCLUSION

Our main goal is an exploratory study of a rigorous method to treat exchange effects in nucleus-nucleus scattering. Starting from a three-body model, we have derived local and nonlocal kernels in a coupled-channel formalism. This represents a natural extension of the three-body CDCC method. The coupled-channel system, involving nonlocal potentials, is solved with the R-matrix theory, associated with the Lagrange-mesh technique. This permits fast and accurate calculations of the scattering matrices and of the cross sections.

We have applied the formalism to typical reactions: $^{13}C + ^{12}C$, $^{13}N + ^{12}C$, and $^{16}O + ^{12}C$, which illustrate the transfer of a neutron, of a proton, and of an α particle, respectively. In each case we started from a core-core optical potential, taken from the literature, and which fits $^{12}C + ^{12}C$ elastic-scattering data. As expected, exchange effects lead to a backward-angle enhancement of the elastic cross sections. For the core-valence potential, we have two "natural" choices: either it is fitted on the spectroscopic properties of the heavy particle, or it is fitted on scattering properties. The first choice guarantees the symmetry of the scattering matrix, since the same Hamiltonian is used in the entrance and exit channels. With our examples, we have however shown that both options provide similar cross sections. This can be explained by the weak contribution of this potential to the nonlocal kernel.

We have shown in Sec. IV that the bound-state wave functions of the $C + v$ system need to be accurately determined up to large distances. If not, the calculation of the various kernels is inaccurate, and the scattering matrices are unstable. For this reason, CDCC calculations involving continuum states raise numerical difficulties with pseudostates as they tend to zero at very large distances only. The use of bins would be preferable. In our applications, however, the binding energies of the projectile are large, and no strong continuum effects are expected.

The present work opens the path to more ambitious calculations, such as the $\alpha + ^8$Be system, where exchange effects could affect the existing calculations [11]. Also it could be extended to more complicated systems, such as $d + ^{11}$Be or $^{13}N + ^{13}C$ which require a four-body theory. Another application of the formalism deals with coupled reaction channel calculations where similar nonlocal kernels are involved [21].

ACKNOWLEDGMENTS

This work was supported by the Fonds de la Recherche Scientifique - FNRS under Grant Nos. 4.45.10.08 and J.0049.19. It benefited from computational resources made available on the Tier-1 supercomputer of the Fédération Wallonie-Bruxelles, infrastructure funded by the Walloon Region under Grant Agreement No. 1117545.

APPENDIX: CALCULATION OF THE NONLOCAL KINETIC ENERGY

The kinetic-energy kernel $\mathcal{T}^{J\pi}_{cL,c'L'}$ is implicitly defined by

$$\int \mathcal{T}^{J\pi}_{cL,c'L'}(R,R')g^{J\pi}_{c'L'}(R')dR' = R\left\langle \varphi^{JM\pi}_{cL} \middle| T_R \middle| \varphi^{JM\pi}_{c'L'} \frac{g^{J\pi}_{c'L'}(R')}{R'} \right\rangle, \quad \text{(A1)}$$

where the integration is performed over $\boldsymbol{r}$ and Ω_R. An explicit expression for this kernel can be obtained by, first, writing the kinetic-energy operator $T_{\boldsymbol{R}}$ in spherical coordinates,

$$T_{\boldsymbol{R}} = -\frac{\hbar^2}{2\mu R}\frac{d^2}{dR^2}R + \frac{\hat{L}^2_{\boldsymbol{R}}}{2\mu R^2}, \tag{A2}$$

where $\hat{L}_{\boldsymbol{R}}$ is the orbital angular momentum associated with the coordinate $\boldsymbol{R}$. The radial part of T_R can be moved outside the matrix element since the function $\varphi^{JM\pi}_{cL}$ is independent of R and since the matrix element does not involve any integration over the coordinate R. Besides, since the operator $\hat{L}^2_{\boldsymbol{R}}$ is Hermitian, it can be applied, with a trivial effect, on the bra. We therefore obtain

$$R\left\langle \varphi^{JM\pi}_{cL}\left| T_{\boldsymbol{R}}\right| \varphi^{JM\pi}_{c'L'}\frac{g^{J\pi}_{c'L'}(R')}{R'}\right\rangle = -\frac{\hbar^2}{2\mu}\left[\frac{d^2}{dR^2} - \frac{L(L+1)}{R^2}\right]R\left\langle \varphi^{JM\pi}_{cL}\left| \varphi^{JM\pi}_{c'L'}\frac{g^{J\pi}_{c'L'}(R')}{R'}\right\rangle \tag{A3}$$

$$= \int\left\{-\frac{\hbar^2}{2\mu}\left[\frac{\partial^2}{\partial R^2} - \frac{L(L+1)}{R^2}\right]\mathcal{N}^{J\pi}_{cL,c'L'}(R,R')\right\}g^{J\pi}_{c'L'}(R')dR', \tag{A4}$$

where the definition (18) of the norm kernel and the Leibniz integral rule have been used. By comparison of Eqs. (A1) and (A4), we get the relation (25), linking the kinetic-energy and norm kernels,

$$\mathcal{T}^{J\pi}_{cL,c'L'}(R,R') = -\frac{\hbar^2}{2\mu}\left[\frac{\partial^2}{\partial R^2} - \frac{L(L+1)}{R^2}\right]\mathcal{N}^{J\pi}_{cL,c'L'}(R,R'). \tag{A5}$$

[1] H. Feshbach, Ann. Rev. Nucl. Sci. **8**, 49 (1958).
[2] W. H. Dickhoff and R. J. Charity, Prog. Part. Nucl. Phys. **105**, 252 (2019).
[3] G. H. Rawitscher, Phys. Rev. C **9**, 2210 (1974).
[4] M. Kamimura, M. Yahiro, Y. Iseri, S. Sakuragi, H. Kameyama, and M. Kawai, Prog. Theor. Phys. Suppl. **89**, 1 (1986).
[5] N. Austern, Y. Iseri, M. Kamimura, M. Kawai, G. Rawitscher, and M. Yahiro, Phys. Rep. **154**, 125 (1987).
[6] M. Yahiro, T. Matsumoto, K. Minomo, T. Sumi, and S. Watanabe, Prog. Theor. Phys. Supp. **196**, 87 (2012).
[7] T. Matsumoto, E. Hiyama, K. Ogata, Y. Iseri, M. Kamimura, S. Chiba, and M. Yahiro, Phys. Rev. C **70**, 061601(R) (2004).
[8] P. Descouvemont, Phys. Rev. C **97**, 064607 (2018).
[9] R. de Diego, J. M. Arias, J. A. Lay, and A. M. Moro, Phys. Rev. C **89**, 064609 (2014).
[10] V. Pesudo, M. J. G. Borge, A. M. Moro, J. A. Lay, E. Nácher, J. Gómez-Camacho, O. Tengblad, L. Acosta, M. Alcorta, M. A. G. Alvarez, C. Andreoiu, P. C. Bender, R. Braid, M. Cubero, A. Di Pietro, J. P. Fernández-García, P. Figuera, M. Fisichella, B. R. Fulton, A. B. Garnsworthy, G. Hackman, U. Hager, O. S. Kirsebom, K. Kuhn, M. Lattuada, G. Marquínez-Durán, I. Martel, D. Miller, M. Moukaddam, P. D. O'Malley, A. Perea, M. M. Rajabali, A. M. Sánchez-Benítez, F. Sarazin, V. Scuderi, C. E. Svensson, C. Unsworth, and Z. M. Wang, Phys. Rev. Lett. **118**, 152502 (2017).
[11] K. Ogata, M. Kan, and M. Kamimura, Prog. Theor. Phys. **122**, 1055 (2009).
[12] P. Descouvemont, Phys. Lett. B **772**, 1 (2017).
[13] W. von Oertzen, Nucl. Phys. A **148**, 529 (1970).
[14] B. Imanishi and W. von Oertzen, Phys. Rep. **155**, 29 (1987).
[15] P. Buttle and L. Goldfarb, Nucl. Phys. **78**, 409 (1966).
[16] J.-M. Sparenberg, D. Baye, and B. Imanishi, Phys. Rev. C **61**, 054610 (2000).
[17] P. Descouvemont and D. Baye, Rep. Prog. Phys. **73**, 036301 (2010).
[18] D. Baye, Phys. Rep. **565**, 1 (2015).
[19] J. Dohet-Eraly, Eur. Phys. J. Plus **132**, 362 (2017).
[20] S. Cotanch, Phys. Lett. B **57**, 123 (1975).
[21] G. R. Satchler, *Direct Nuclear Reactions* (Oxford University Press, Oxford, 1983).
[22] I. J. Thompson, Comput. Phys. Rep. **7**, 167 (1988).
[23] Shubhchintak and P. Descouvemont, Phys. Rev. C **100**, 034611 (2019).
[24] L. F. Canto and M. S. Hussein, *Scattering Theory of Molecules, Atoms and Nuclei* (World Scientific Publishing, Singapore, 2013).
[25] Nguyen Tri Toan Phuc, N. H. Phuc, and D. T. Khoa, Phys. Rev. C **98**, 024613 (2018).
[26] N. H. Phuc, D. T. Khoa, and N. T. T. Phuc, Eur. Phys. J. A **57**, 7 (2021).
[27] Nguyen Tri Toan Phuc, R. S. Mackintosh, N. H. Phuc, and D. T. Khoa, Phys. Rev. C **100**, 054615 (2019).
[28] E. Liénard, D. Baye, T. Delbar, P. Descouvemont, P. Duhamel, W. Galster, M. Kurokawa, P. Leleux, I. Licot, P. Lipnik, C. Michotte, T. Motobayashi, A. Ninane, J. Vanhorenbeeck, and J. Vervier, Phys. Rev. C **52**, 775 (1995).
[29] H. Voit, N. Bischof, W. Tiereth, I. Weitzenfelder, W. von Oertzen, and B. Imanishi, Nucl. Phys. A **476**, 491 (1988).
[30] B. Imanishi, V. Denisov, and T. Motobayashi, Phys. Rev. C **55**, 1946 (1997).
[31] D. Baye, Nucl. Phys. A **460**, 581 (1986).
[32] W. Treu, H. Fröhlich, W. Galster, P. Dück, and H. Voit, Phys. Rev. C **22**, 2462 (1980).
[33] W. von Oertzen and B. Imanishi, Nucl. Phys. A **424**, 262 (1984).
[34] A. J. Koning and J. P. Delaroche, Nucl. Phys. A **713**, 231 (2003).
[35] H. Fröhlich, N. Bischof, W. Tiereth, H. Voit, W. von Oertzen, and B. Imanishi, Nucl. Phys. A **420**, 124 (1984).
[36] A. C. C. Villari, A. Lépine-Szily, R. L. Filho, O. P. Filho, M. M. Obuti, J. M. Oliveira, Jr., and N. Added, Nucl. Phys. A **501**, 605 (1989).
[37] N. Oulebsir, F. Hammache, P. Roussel, M. G. Pellegriti, L. Audouin, D. Beaumel, A. Bouda, P. Descouvemont, S. Fortier,

L. Gaudefroy, J. Kiener, A. Lefebvre-Schuhl, and V. Tatischeff, Phys. Rev. C **85**, 035804 (2012).
[38] M. Avrigeanu, A. Obreja, F. Roman, V. Avrigeanu, and W. von Oertzen, At. Data Nucl. Data Tables **95**, 501 (2009).
[39] I. Thompson, M. Nagarajan, J. Lilley, and M. Smithson, Nucl. Phys. A **505**, 84 (1989).
[40] R. S. Mackintosh, Eur. Phys. J. A **55**, 147 (2019).
[41] M. Abramowitz and I. A. Stegun, *Handbook of Mathematical Functions* (Dover, London, 1972).
[42] P. Buttle and L. Goldfarb, Nucl. Phys. A **115**, 461 (1968).
[43] F. Perey and B. Buck, Nucl. Phys. **32**, 353 (1962).